Monolithic 3-D Silicon Photonics

Prakash Koonath, Tejaswi Indukuri, and Bahram Jalali, *Fellow, IEEE*

***Abstract*—A monolithic CMOS compatible process has been developed to realize vertically integrated devices in silicon. The method involves the implantation of an oxygen into a patterned silicon substrate to form buried guiding structures. These buried devices are separated from a surface silicon layer by an intervening layer of silicon dioxide formed through the implantation process. Photolithography and etching is used to define devices on the surface silicon layer. The method has been utilized to realize the vertically coupled microdisk resonators and a variety of microresonator-based integrated optical elements. A new method for extraction of the unloaded Q of a cavity from its measured spectrum is also described.**

***Index Terms*—Cavity resonator filters, integrated optics, microresonators, monolithic integrated circuits, silicon-on-insulator (SOI) technology.**

I. Introduction

SILICON-ON-INSULATOR (SOI) material system has proven to be an efficient platform for the realization of both electronic and photonic devices. Recent years have seen a significant amount of research in the area of silicon photonics, resulting in the demonstration of a variety of optical functionalities, including multimode interference (MMI) couplers, arrayed waveguide gratings (AWGs), nanowires, microresonators, optical modulators, wavelength converters, Raman amplifiers, and lasers [1]–[16]. One of the most attractive features of the SOI material system is the prospect of a full integration of the optical and electronic devices on the same substrate. However, the increasing importance of a real estate on silicon substrates necessitates the development of innovative fabrication technologies that would make the integration of the optical and electronic devices viable on these substrates, without compromising the real-estate economics of the wafer manufacturing. In order to take advantage of the foundry capabilities in silicon, it is preferable that these new technologies be compatible with the well-established CMOS processing techniques.

Vertical integration of devices on a chip is an efficient way to fabricate densely integrated three-dimensional (3-D) structures, thereby enhancing the functionality of the chip. Apart from this inherent advantage, in the realization of the optical waveguiding structures, vertical integration offers the prospect of a precise control of a coupling coefficient in vertically coupled devices [17], [18]. Here, the control over the critical dimension is more precise than laterally patterned structures, where the limits are set by the photolithography. Thus, a complex optical circuitry with accurately controlled evanescent coupling between devices is possible by employing vertically integrated optical devices.

We have previously demonstrated the process of separation by implantation of oxygen (SIMOX) 3-D sculpting, to realize three-dimensionally integrated optical devices in silicon. A variety of optical devices including buried waveguides, vertically coupled microdisk resonators and add-drop multiplexers have been realized using this technique [19]–[22].

In this paper, we begin by reviewing the process of the SIMOX 3-D sculpting and the synthesis of buried waveguides and waveguide coupled microdisk resonators. We then present new results on 1) passband flattened filters consisting of multistage vertically coupled microdisk resonators, 2) microdisk-based Vernier filters, and 3) a new technique for extracting the unloaded Q of a resonator from the measurements of its spectrum.

II. Process of SIMOX 3-D Sculpting

The SIMOX process involves the implantation of oxygen ions into a silicon substrate, followed by a high-temperature anneal (around 1300 °C) of the substrate in order to cure the implantation damage and to effect an SiO_2 formation. The thickness and the depth of the buried oxide layer are, respectively, determined by the implantation dose and energy. It has been observed that in order to achieve a good quality buried oxide and to keep the defect densities in the range of $< 10^5/\text{cm}^2$, the implantation dose should be in the range of $1 \times 10^{17} - 9 \times 10^{17}$ ions/cm^2, with implantation energies in the range of 40–200 KeV [23]. The process is conventionally used to obtain thin silicon layers (of the order of 3000 Å) on top of a buried oxide layer of thickness of the same order of magnitude. There has been an attempt previously to fabricate 3-D structures in SOI wafers using the SIMOX process, combining it with epitaxial growth of silicon [24]. The complete process involved two implantation steps and two epitaxial growths in order to grow vertically integrated SOI waveguides. The waveguides fabricated in this case were planar in nature with the guiding layer thickness of the order of 2 μm.

A method, utilizing the implantation of oxygen ions into a masked SOI substrate, is employed to realize buried rib waveguides. Fig. 1 depicts the process flow of the fabrication of vertically integrated structures using the technique of SIMOX 3-D sculpting. Implantation of oxygen ions is performed on an SOI substrate that has been patterned with a thermally grown oxide. The thickness of the oxide mask may be chosen suitably to decelerate the oxygen ions that penetrate into the area underneath the mask. The angled sidewall of the buried rib waveguide formed after the high-temperature anneal arises

Manuscript received August 17, 2005. This work was performed under the chip scale (CS)-WDM program funded by the Microsystems Technology Office (MTO) of the Defense Advanced Research Projects Agency (DARPA).

The authors are with the Department of Electrical Engineering, University of California, Los Angeles, CA 90095-1594 USA.

Digital Object Identifier 10.1109/JLT.2006.871121

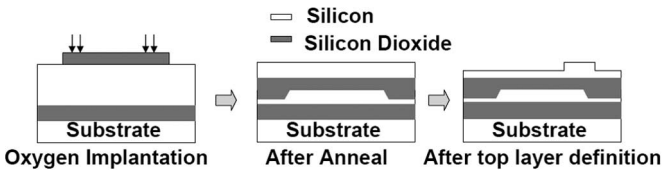

Fig. 1. Process flow of a SIMOX 3-D sculpting.

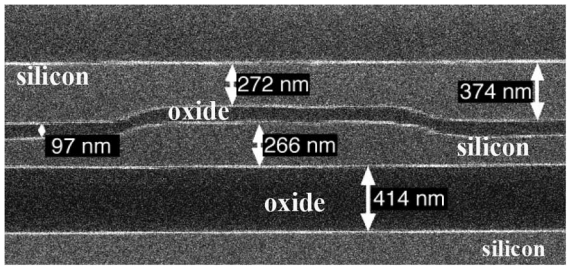

Fig. 2. Cross-sectional SEM view of the buried rib waveguide formed by the process of a SIMOX 3-D sculpting.

due to the lateral straggle of the implanted oxygen ions. After the anneal, devices may be defined on the top layer using a conventional lithography and etching process, as shown in Fig. 1.

III. Fabrication of Devices

An SOI wafer [made by Silicon-On-Insulator Technologies (SOITEC) Inc.] with 0.6 μm of silicon on top of a buried oxide layer of 1.0 μm thickness was oxidized and patterned using a reactive-ion-etching process to form oxide stripes of thickness 0.06 μm and of width 2 μm. The patterned wafer was then implanted with oxygen ions with a dose of 5×10^{17} ions/cm^2 at energy of 150 KeV. The implanted wafers were then annealed at 1320 °C for 7.5 h in an ambient of Argon, with 1% oxygen, to cure the implantation damage. Fig. 2 shows the SEM photograph of a buried rib waveguide structure that was fabricated employing the technique of SIMOX 3-D sculpting, dimensions of which are shown in the figure. It may be seen from the figure that the process has resulted in the formation of submicrometer rib waveguides in the bottom silicon layer, separated from the continuous silicon layer on the top by the oxide layer formed after the oxygen implantation and subsequent anneal. The buried oxide that was formed after the implantation and anneal is found to be uniform, which is very important in achieving accurate control of the evanescent coupling from the rib waveguides to the devices on the top silicon layer. It has been observed that, under nonideal conditions, the SIMOX process can result in the formation of a high density of silicon islands inside the buried oxide [25]. The optimized SIMOX process employed in this paper has been successful in preventing the formation of these islands that degrade the quality of the buried oxide. Measurements based on a cutback technique reveal that these buried waveguides have propagation losses of around 4 dB/cm.

In order to fabricate the microdisk resonators on the top silicon layer, a silicon-nitride layer of thickness 0.1 μm was deposited, and patterned using standard lithography and reactive-ion etching to form circular discs of desired dimensions. The substrate was then oxidized to remove the silicon on the surface layer, everywhere except underneath the circular silicon-nitride disks. This results in the formation of a microdisk structure on the surface silicon layer that is coupled vertically to the rib waveguides in the buried silicon layer through the oxide layer formed after the oxygen implantation. This technique has been utilized to realize a variety of vertically coupled devices that are described in the following sections.

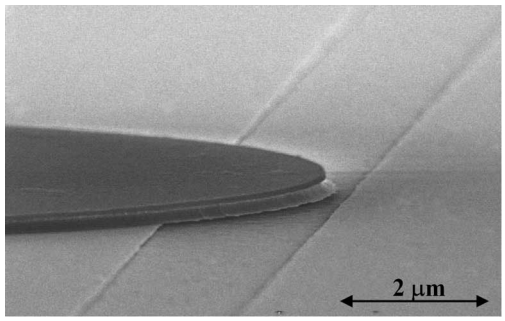

Fig. 3. SEM picture of the fabricated microdisk resonators of radius 23 μm on the top silicon layer with bus waveguides underneath.

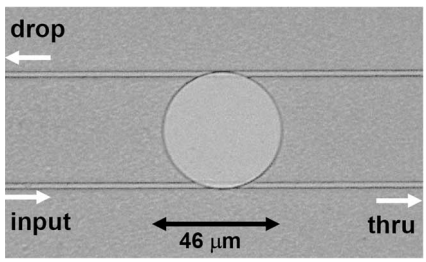

Fig. 4. Top view of a microdisk resonator vertically coupled to bus waveguides.

IV. Characterization of Devices

A. Vertically Coupled Microdisk Resonators

Fig. 3 shows the SEM photograph of a microdisk resonator fabricated on the surface layer silicon, straddling the buried bus waveguide. The silicon-nitride disk used as the oxidation mask is also seen in the picture, on top of the microdisk. It may be noted here that the silicon dioxide that was formed after the oxidation, and the buried oxide layer formed during the implantation, were removed to obtain SEM photographs that clearly illustrate the structure of the device. The optical micrograph in Fig. 4 shows the top view of the fabricated device.

Fig. 5 shows the experimental setup used to characterize the fabricated microdisk resonators. Unpolarized light from an amplified spontaneous emission (ASE) source was passed through an inline fiber polarizer (General Photonics make, Extinction Ratio 40 dB) and a polarization controller (General Photonics make, Extinction Ratio 40 dB), which can rotate the state of polarization of the light to any desired state. This polarized light was then coupled into the bus waveguides using a tapered fiber that has a spot diameter of 2 μm. The light

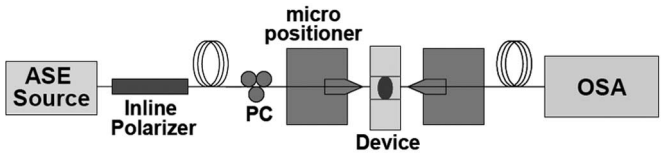

Fig. 5. Experimental setup used to characterize the microdisk resonators.

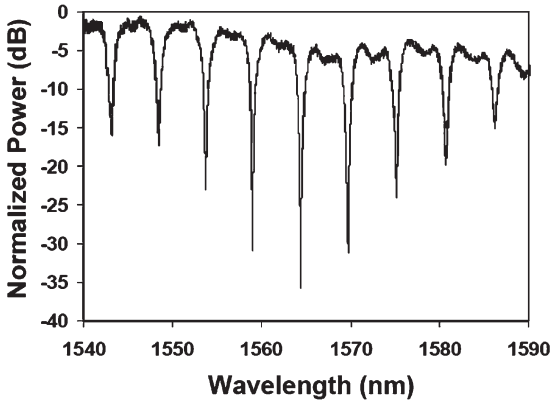

Fig. 6. Throughput port transmission characteristics of the microdisk resonator.

output from the drop ports of the filter was collected using a tapered fiber, similar to the one used at the input. The fiber-to-fiber insertion loss of this setup was found to be ~ 30 dB. This includes the mode mismatch loss and reflection losses at the input and the output facets of the device and the propagation losses in the waveguides. The collected light was observed using an optical spectrum analyzer (ANDO Model: 6319) that can measure power levels as low as 1 pW. This setup was used to characterize other optical devices described in this paper as well. Fig. 6 shows the throughput port responses of the filters, characterized by launching optical power at the input port (see Fig. 4) and observing the optical spectra at the throughput port. The spectrum displayed in Fig. 6 is normalized with respect to the maximum transmission of the throughput port after correcting for the spectral shape of the ASE source. Sharp resonances are observed with a free spectral range (FSR) of around 5.4 nm, with the narrowest resonance observed showing a full-width at half-maximum (FWHM) of 1.16 nm, centered at 1564 nm. This corresponds to a loaded quality factor, Q, of around 1350, with a suppression value greater than 30 dB for the resonant wavelength at the throughput port. Measured value of Q in this device is limited by the loading of the resonator since the microdisk is separated from the bus waveguides through the intervening silicon-dioxide layer of thickness only ~ 100 nm.

We have developed a mathematical formalism to extract the intrinsic quality factor $Q_{\mathrm{intrinsic}}$ of a microresonator by measuring the

1) loaded quality factor Q of the resonator in a symmetrically loaded configuration, as shown in Fig. 4;
2) extinction ratio observed in its throughput transmission spectrum.

The details of this formalism are given in the Appendix. It is seen that extinction ratio ER around a resonance of the

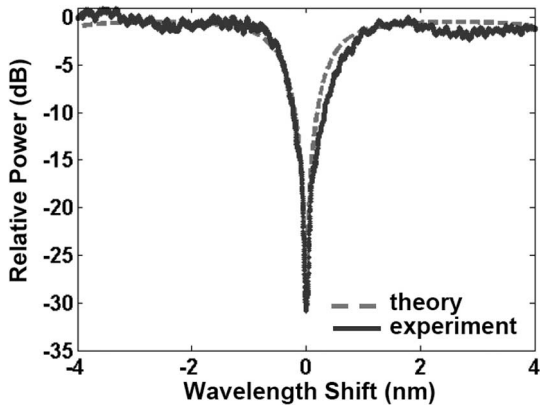

Fig. 7. Comparison of the experimental data with theory for the microdisk resonance at 1564.3 nm.

microresonator may be related to the Q of the device by the expression given by (1) as

$$\mathrm{ER} = \left[\frac{(1-\kappa)^2 - 2\cdot(1-\kappa)\cdot\sqrt{G}+G}{(1-\kappa)^2 + 2\cdot(1-\kappa)\cdot\sqrt{G}+G}\right]\times\left[\frac{1+G+2\cdot\sqrt{G}}{1+G-2\cdot\sqrt{G}}\right] \tag{1}$$

where κ is the power coupling coefficient between one of the bus waveguides and the microdisk resonator, and G is the round-trip power gain inside the cavity. G is related to the Q as

$$G = \exp\left(-\frac{\omega_0 T_{\mathrm{r}}}{Q}\right) \tag{2}$$

where ω_0 is the angular resonant frequency and T_{r} is the round-trip time inside the cavity. Thus, by measuring the extinction ratio and the Q of the resonator, κ may be extracted from (1). Once κ is known, the quality factor associated with the I/O coupling Q_{coupling}, may be determined by the relation

$$Q_{\mathrm{coupling}} = \frac{\omega_0 T_{\mathrm{r}}}{\ln\left(\frac{1}{1-\kappa}\right)} \tag{3}$$

and we can estimate $Q_{\mathrm{intrinsic}}$ of the resonator using

$$\frac{1}{Q} = \frac{2}{Q_{\mathrm{coupling}}} + \frac{1}{Q_{\mathrm{intrinsic}}}. \tag{4}$$

The factor of 2 in (4) arises from the fact that we assume a symmetrically coupled microresonator (same value of κ at both the input and drop-port coupling), which is true for the devices explored in this paper.

From the throughput spectrum obtained in Fig. 6, the resonator shows a loaded Q of 1350 at the resonance wavelength 1564.3 nm, with an extinction ratio of 30.2 dB. Based on the formalism outlined in the Appendix, we estimate the power coupling coefficient κ to be 0.45 for this case. Fig. 7 shows the experimentally observed resonance at 1564.3 nm, plotted along with the theoretical curve generated using the (A5) given in the Appendix. It may be seen that there is good agreement between the experimentally observed spectrum and the theoretical

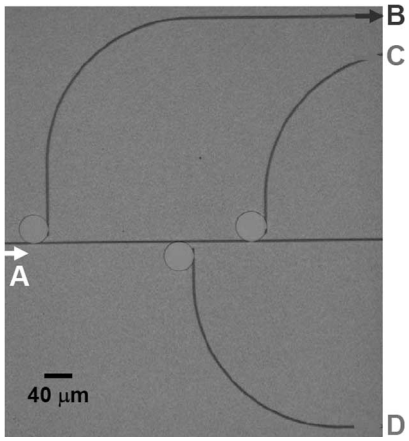

Fig. 8. Top view of the fabricated 1 × 3 add-drop multiplexer using disks of radii 20, 20.5, and 21 μm.

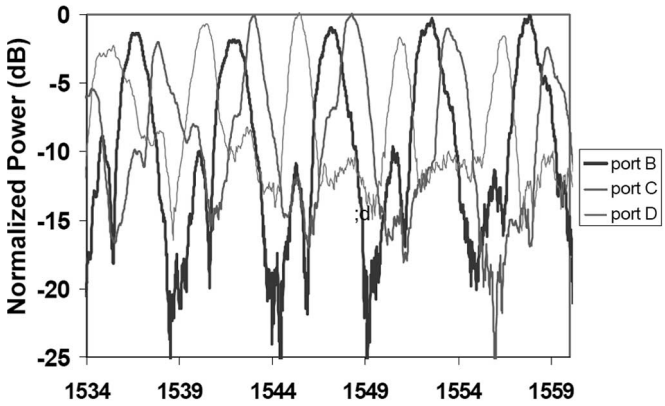

Fig. 9. Drop-port optical spectra of the 1 × 3 add-drop filter.

plot. The estimated value of $Q_{\mathrm{intrinsic}}$ of the device is around 4.5×10^4 at this wavelength.

B. Add-Drop Multiplexers

The process described in the previous section was used to realize add-drop multiplexers utilizing vertically coupled microdisk resonators. Fig. 8 shows the top view of a 1 × 3 drop filter fabricated using this process. Disks of radii 20, 20.5, and 21 μm were used to obtain resonators with slightly shifted resonance wavelengths for these resonators. Fig. 9 shows the drop-port responses of the filters, characterized by launching an optical power at port A and observing the drop-port optical spectra at ports B, C, and D. Fabricated disks show a FSR of around 5 nm. The adjacent channel wavelength separation between port B and port C is approximately 1.0 nm, whereas that of port B and port D is around 1.5 nm. The average value of adjacent channel crosstalk suppression, over the wavelength band of 1534–1560 nm, was found to be 12.1 dB for channels dropped at port D. At ports B and C, these values were found to be 8.3 and 6.2 dB, respectively.

C. Cascaded Microdisk Resonators

It has been demonstrated that cascaded resonator structures may be utilized to improve the filter characteristics of devices employing microcavities, including the flatness of the passband, the sharpness of the rolloff from the passband to the stopband and the suppression of adjacent channel crosstalk [26], [27]. The SIMOX 3-D sculpting has been utilized to fabricate devices that consist of two microdisk resonators vertically coupled to each other through the oxide layer formed after the implantation and subsequent anneal. The resonators themselves are coupled to bus waveguides that act as the input and output ports of the device. Fig. 10 represents a schematic of the device showing the vertically coupled microresonators and the bus waveguides, with the arrows indicating the direction of flow of light through these devices.

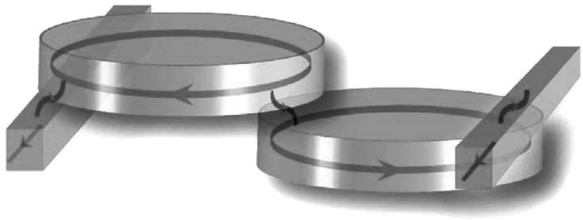

Fig. 10. Three-dimensional schematic of vertically coupled microdisk resonators and bus waveguides illustrating the flow of an optical energy.

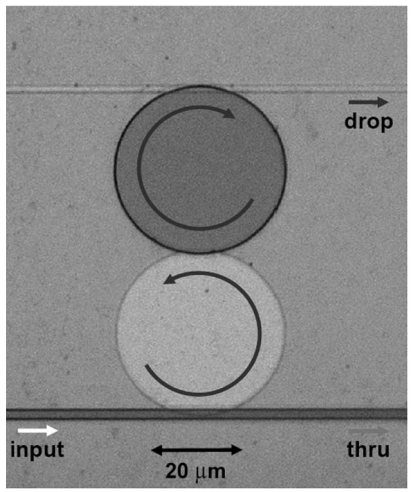

Fig. 11. Top view of the vertically coupled cascaded microdisk resonators.

It may be emphasized here that we have realized waveguides as well as microdisk structures on both layers of the silicon, coupled vertically through an intervening layer of SiO_2. These devices distinctly demonstrate the capability of the SIMOX 3-D sculpting to engineer 3-D structures in the silicon (the intervening layer of oxide through which the coupling of light takes place is omitted in Fig. 10 for the simplicity of illustration). Fig. 11 shows the top view of the fabricated two-stage device with cascaded microdisks of radius 20 μm, coupled to bus waveguides of width 2 μm. When the optical energy is introduced to the input port of the device, resonant wavelengths are transmitted to the drop port, after traversing through the cascaded disk structure. Fig. 12 shows the drop-port transmission response, characterized by launching the optical power at an input port and collecting the optical spectra at the drop port of the device. Fabricated disks show a FSR of around 5.7 nm, with maximum extinction ratios $\sim$ 12 dB. A comparison of

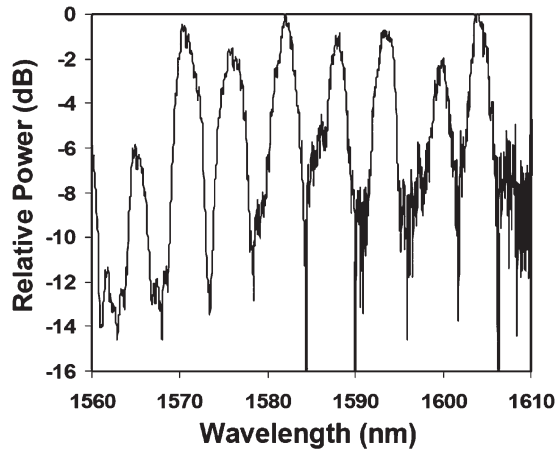

Fig. 12. Drop-port resonance characteristics of the cascaded device.

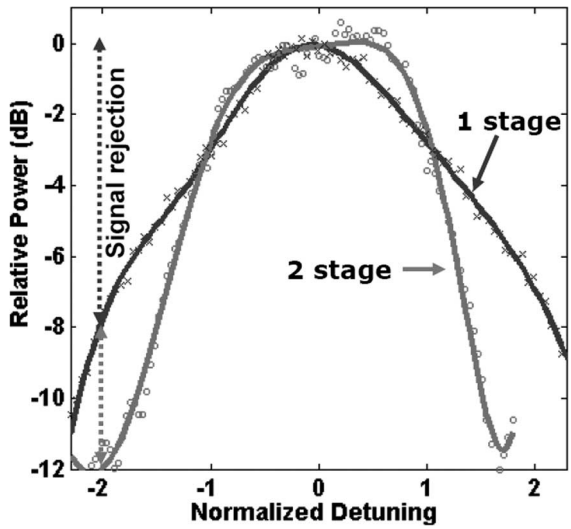

Fig. 13. Comparison of the filter characteristics of the two-stage device with a single-stage device, with frequency scale normalized to 3-dB bandwidths.

the performance of the two-stage device to that of a single-stage device, as shown in Fig. 13, illustrates the superior characteristics of the two-stage resonator in terms of its steeper rolloff, better out-of-band rejection, and flatter passband. Note that the frequency scale in this figure is normalized to the 3-dB bandwidths of the individual filters. The shape factor, which is a measure of the flatness of the passband [27], defined as the ratio of the -1-dB bandwidth to the -10-dB bandwidth, is 0.47 for the two-stage device, compared to a value of 0.22 for the single-stage device. Also, at twice the value of the 3-dB bandwidth, the two-stage device shows a 4-dB improvement in the out-of-band signal rejection over the single-stage device. It may be noted that the single-stage device used for the purpose of this comparison is fabricated on the same chip as that of the two-stage device.

D. Vernier Filters

Vernier filters are frequently employed in the synthesis of optical filters to increase their FSR [27]. Filters with wide

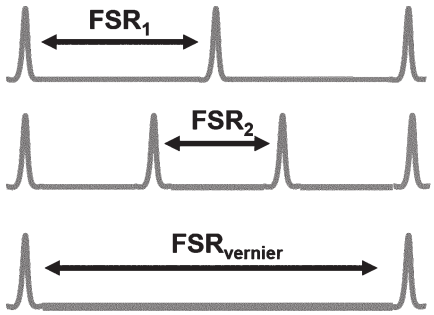

Fig. 14. Schematic depiction of the increase in FSR of a filter using vernier architecture.

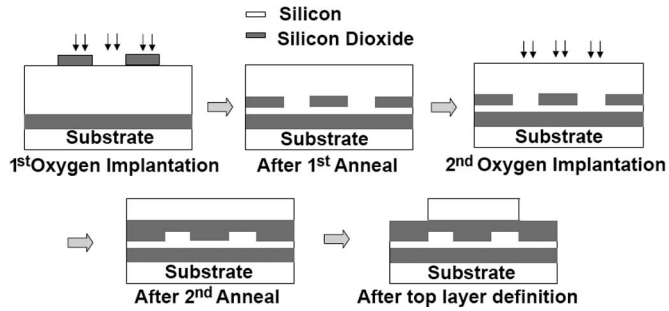

Fig. 15. Process flow of the modified SIMOX 3-D sculpting process for the fabrication of vernier filters.

FSRs are essential to wavelength division multiplexing (WDM) networks that accommodate a large number of channels. Microresonator-based vernier filters may be realized by cascading two resonators of different radii. The transfer function at the drop port of the cascaded device is expressed as a product of the transfer functions of the individual filters, resulting in an increase in the FSR of the combined device, as depicted in Fig. 14.

We have explored a modified version of the SIMOX 3-D sculpting technique, employing two implantation steps, in the fabrication of these vernier filters. The process flow is, as shown in Fig. 15. Implantation of oxygen ions is performed on an SOI substrate that is patterned with thermally grown oxide. In this case, the oxide mask is made thick enough to completely prevent the oxygen ions from penetrating into the silicon substrate underneath the mask. After this first implantation step, the wafer is annealed to cure the implantation damage, which also results in the formation of a buried oxide layer everywhere, except in those regions underneath the thermal oxide mask, as shown in Fig. 15. Subsequently, the thermal oxide mask is removed and the wafer undergoes another implantation, at a lower energy, and annealing to form buried rib waveguides in the lower layer separated from the top layer by the oxide layer formed through the implantation. As done previously, microdisks are defined on the top layer using a lithography and etching process.

An SOI wafer (made by SOITEC Inc.) with 1.050 μm of silicon on top of a buried oxide layer of 1.0 μm thickness was oxidized and patterned using reactive-ion-etching process to form oxide stripes of thickness 1.00 μm and of width 2 μm. The patterned wafer was then implanted with oxygen

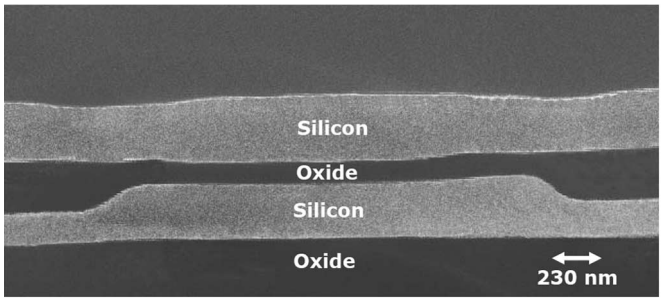

Fig. 16. Cross-sectional SEM view of the buried rib waveguide formed by a SIMOX 3-D sculpting employing two implantation steps.

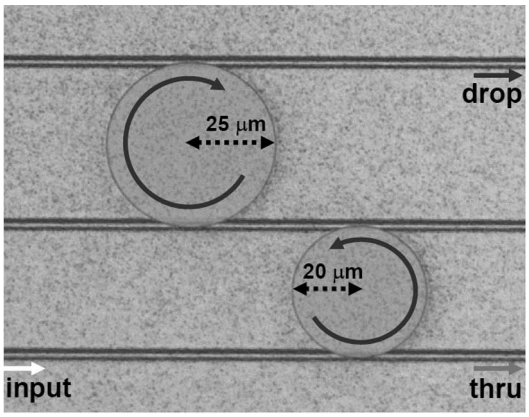

Fig. 17. Vernier filters made using microresonators of radii 20 and 25 μm.

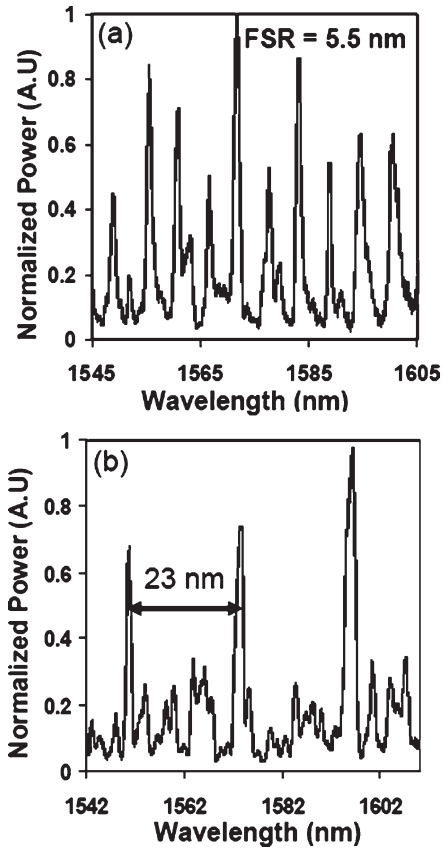

Fig. 18. Drop-port characteristics of (a) device consisting of cascaded microdisks with identical radii [20 μm] and (b) vernier filters made using microdisks of radii 20 and 25 μm.

ions with a dose of 5×10^{17} ions/cm^2 at an energy of 150 KeV. The implanted wafers were then annealed under the same conditions described in Section III. This wafer then undergoes another implantation step, with oxygen ions with a dose of 5×10^{17} ions/cm^2, at an energy of 110 KeV and subsequent high temperature anneal.

Fig. 16 shows the SEM photograph of a buried rib waveguide structure that was fabricated employing this process, dimensions of which are shown in the figure. It may be seen from the figure that the process has resulted in the formation of rib waveguides in the bottom silicon layer, separated from the continuous silicon layer on the top by the oxide layer formed after the oxygen implantation and subsequent anneal. The nonuniformities observed in the top layer silicon arise due to the volume expansion of SiO_2 after the first implantation step. Fig. 17 shows the top view of the fabricated two-stage device with cascaded microdisks of radius 20 and 25 μm, coupled to bus waveguides of width 2 μm. When the optical energy is introduced to the input port of the device, wavelengths that are resonant with both the resonators are transmitted to the drop port, after traversing through the cascaded disk structure. Fig. 18(a) shows the drop-port transmission response of a filter with microdisk resonators of identical radii (20 μm) compared the drop-port spectra of a vernier filter in Fig. 18(b). The vernier filter has an FSR of 23 nm compared to that of the 5.5-nm FSR observed in Fig. 18(a) for the device with disks of identical radii (20 μm). Thus, the effective FSR has been increased by more than a factor of 4, by employing vernier filters.

V. Discussion and Summary

In this paper, a novel method (SIMOX 3-D sculpting) to realize vertically integrated device structures in silicon has been discussed. The method of the SIMOX 3-D sculpting is based on a modified version of the conventional SIMOX process. Two different approaches have been explored in this paper to obtain devices on vertically stacked layers of silicon separated by the silicon-dioxide layer formed through the process of implantation. A number of integrated optical devices, including buried waveguides, vertically coupled microdisk resonators, add-drop filters, cascaded microdisk resonators, and vernier filters, have been realized. The attractiveness of the process lies in its ability to synthesize 3-D integrated optical device structures in a monolithic fashion. Three-dimensional integration allows for the dense integration of devices that acquires importance in the context of the reduction of a real-estate consumption on a silicon wafer. Apart this advantage, the use of a vertical coupling to inject light into the resonant cavities offers a precise control of the coupling coefficient in these structures. This is possible due to the fact that the critical dimension in vertically coupled device may more precisely be controlled than laterally coupled devices. The offset between the edge of a buried waveguide and the edge of a microdisk resonator is an additional design parameter that may be used in the process developed here to engineer the coupling between the disk and the waveguide. The device characteristics of microresonant cavities depend critically on the photon lifetime in these devices. Thus, the control

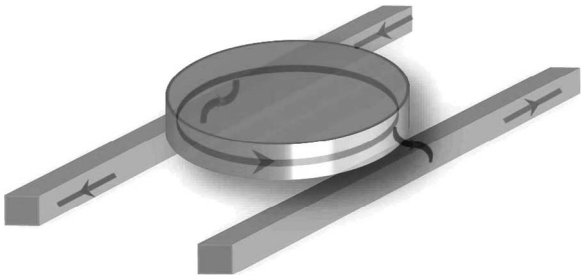

Fig. 19. Three-dimensional schematic of a microdisk resonators vertically coupled to bus waveguides illustrating the flow of optical energy.

over the coupling coefficient acquires considerable importance in the context of designing devices based on microresonant cavities. It is evident from the description of the formation of buried waveguides by the SIMOX 3-D sculpting process in Section III that the oxide layer formed by the implantation separates two vertically stacked layers of silicon. Thus, if optical devices are confined to the buried silicon layer, it is then possible to realize MOS transistors on the top silicon layer, facilitating the fabrication of optical and electronic devices on the same substrate. This is a significant advantage in the migration towards optical interconnects in silicon. For the integration of optical interconnects with electronic chips, it is desirable to realize optical interconnects in such a way that they consume the least amount of real estate on the silicon wafer. The SIMOX 3-D sculpting provides an approach that may possibly be used to monolithically integrate optical and electronic devices on the same substrate without compromising the real-estate economics of wafer manufacturing.

APPENDIX

The mathematical formalism used to extract the intrinsic quality factor $Q_{\mathrm{intrinsic}}$ of a microresonator, symmetrically coupled to two bus waveguides, is developed in this section. The analysis closely follows the formalism developed in [28] to analyze the resonance properties of passive optical cavities. Fig. 19 shows the schematic of a microresonator vertically coupled to two bus waveguides.

The loaded quality factor Q of a resonator may be related to the quality factor associated with the input/drop-port coupling Q_{coupling} and $Q_{\mathrm{intrinsic}}$ as [17]

$$\frac{1}{Q} = \frac{1}{Q_{\mathrm{input-coupling}}} + \frac{1}{Q_{\mathrm{intrinsic}}} + \frac{1}{Q_{\mathrm{drop-coupling}}}. \quad \text{(A1)}$$

For a symmetrically coupled resonator, where the input and drop couplings are equal, this equation reduces to

$$\frac{1}{Q} = \frac{2}{Q_{\mathrm{coupling}}} + \frac{1}{Q_{\mathrm{intrinsic}}}. \quad \text{(A2)}$$

If Q and Q_{coupling} are known, $Q_{\mathrm{intrinsic}}$ may be calculated using (A2).

Experimentally, the Q of a cavity may be determined by measuring the spectral width $\Delta\lambda$ of a resonance at the resonance wavelength λ_0, using the relation

$$Q = \frac{\lambda_0}{\Delta\lambda}. \quad \text{(A3)}$$

Q_{coupling} is related to the power coupling coefficient κ, between one of the bus waveguides and the microdisk resonator, by the relation [28]

$$Q_{\mathrm{coupling}} = \frac{\omega_0 T_{\mathrm{r}}}{\ln\left(\frac{1}{1-\kappa}\right)} \quad \text{(A4)}$$

where ω_0 is the angular resonant frequency, and T_{r} is the round-trip time inside the cavity. In the analysis that follows, it will be shown that κ may be estimated, and hence $Q_{\mathrm{intrinsic}}$, by measuring the Q and the extinction ratio observed in the throughput spectrum of a resonator.

Let E_{inc}, E_{thru}, and E_{drop} denote the incident, throughput, and dropped complex signal amplitudes, respectively. Let α denote the intensity attenuation coefficient due to the propagation losses inside the cavity. Let ϕ represent the round-trip phase shift acquired by the optical field as it propagates inside the cavity. The net complex round-trip gain (loss) for the field amplitude, for a disk of radius R, is then given by the expression

$$g = (1-\kappa)e^{-i\phi-\alpha\pi R}. \quad \text{(A5)}$$

The round-trip power gain (loss) G is given by

$$G = g^* g = (1-\kappa)^2 e^{-\alpha\cdot 2\pi R} \quad \text{(A6)}$$

where g^* represents the complex conjugate of g. G may be related to the loaded quality factor Q of the resonator by the expression [28]

$$G = \exp\left(-\frac{\omega_0 T_{\mathrm{r}}}{Q}\right). \quad \text{(A7)}$$

E_{thru} is related to E_{inc} by the expression

$$\frac{E_{\mathrm{thru}}}{E_{\mathrm{inc}}} = \frac{[(1-\kappa)-g]}{(1-g)\sqrt{1-\kappa}}. \quad \text{(A8)}$$

The ratio of the optical intensity at the throughput port to the incident intensity is then given by

$$\frac{I_{\mathrm{thru}}}{I_{\mathrm{inc}}} = \left[\frac{1}{1-\kappa}\right]\cdot\left[\frac{(1-\kappa)^2 - 2\cdot(1-\kappa)\cdot\sqrt{G}\cdot\cos\phi + G}{1+G-2\cdot\sqrt{G}\cdot\cos\phi}\right]. \quad \text{(A9)}$$

When the wavelength of the incident field is a resonant wavelength of the resonator, corresponding to $\phi = 2m\pi$, where m is an integer, the incident optical energy is directed to the drop port of the resonator, resulting in a minima for the expression given by (A9). This minimum value is given by

$$\left[\frac{I_{\mathrm{thru}}}{I_{\mathrm{inc}}}\right]_{\min} = \left[\frac{1}{1-\kappa}\right]\cdot\left[\frac{(1-\kappa)^2 - 2\cdot(1-\kappa)\cdot\sqrt{G} + G}{1+G-2\cdot\sqrt{G}}\right]. \quad \text{(A10)}$$

Similarly, the maxima for the expression in (A9) occurs when $\phi = (2m+1)\pi$. The maximum value is given by

$$\left[\frac{I_{\text{thru}}}{I_{\text{inc}}}\right]_{\max} = \left[\frac{1}{1-\kappa}\right] \cdot \left[\frac{(1-\kappa)^2 + 2\cdot(1-\kappa)\cdot\sqrt{G} + G}{1+G+2\cdot\sqrt{G}}\right]. \tag{A11}$$

Taking the ratio of the expressions given in (A10) and (A11), an expression for the extinction ratio observed in the throughput spectrum of the resonator may be obtained as

$$\begin{aligned}\left[\frac{I_{\text{thru(min)}}}{I_{\text{thru(max)}}}\right] &= \text{ExtinctionRatio} \\ &= \left[\frac{(1-\kappa)^2 - 2\cdot(1-\kappa)\cdot\sqrt{G} + G}{(1-\kappa)^2 + 2\cdot(1-\kappa)\cdot\sqrt{G} + G}\right] \\ &\quad \times \left[\frac{1+G+2\cdot\sqrt{G}}{1+G-2\cdot\sqrt{G}}\right]. \end{aligned} \tag{A12}$$

G may be determined from the expression given in (A7) by measuring the Q of the device. Thus, by measuring the extinction ratio in the throughput spectrum of the resonator, and using the expression given in (A12), the power coupling coefficient κ may be determined. This value of κ may be used in (A4) to determine Q_{coupling}. Once Q_{coupling} is known, the intrinsic quality factor $Q_{\text{intrinsic}}$ of the resonator may be determined using the expression given in (A2). (It may be mentioned here that (A12) is quadratic in κ, resulting in two solutions for the value of κ. However, only one of these solutions lead to a physically meaningful value of $Q_{\text{intrinsic}}$.)

ACKNOWLEDGMENT

The authors would like to thank K. Kishima for his assistance. The authors would like to thank Dr. J. Shah of DARPA for his support.

REFERENCES

[1] B. Jalali, S. Yegnanarayanan, T. Yoon, T. Yoshimoto, I. Rendina, and F. Coppinger, "Advances in silicon-on-insulator optoelectronics," *IEEE J. Sel. Topics Quantum Electron. (Special Issue Silicon-Based Optoelectronics)*, vol. 4, no. 6, pp. 938–947, Dec. 1998.

[2] K. Jia, W. Wang, Y. Tang, Y. Yang, J. Yang, X. Jiang, Y. Wu, M. Wang, and Y. Wang, "Silicon-on-insulator-based optical demultiplexer employing turning-mirror-integrated arrayed-waveguide grating," *IEEE Photon. Technol. Lett.*, vol. 17, no. 2, pp. 378–380, Feb. 2005.

[3] T. Tsuchizawa, K. Yamada, H. Fukuda, T. Watanabe, J. Takahashi, M. Takahashi, T. Shoji, E. Tamechika, S. Itabashi, and H. Morita, "Microphotonics devices based on silicon microfabrication technology," *IEEE J. Sel. Topics Quantum Electron.*, vol. 11, no. 1, pp. 232–240, Jan. 2005.

[4] A. Liu, R. Jones, L. Liao, D. Samara-Rubio, D. Rubin, O. Cohen, R. Nicolaescu, and M. Paniccia, "A high-speed silicon optical modulator based on a metal-oxide-semiconductor capacitor," *Nature*, vol. 427, no. 6975, pp. 615–618, Feb. 2004.

[5] O. Boyraz and B. Jalali, "Demonstration of a silicon Raman laser," *Opt. Express*, vol. 12, no. 21, pp. 5269–5273, Oct. 2004.

[6] H. Rong, R. Jones, A. Liu, O. Cohen, D. Hak, A. Fang, and M. Paniccia, "A continuous-wave Raman silicon laser," *Nature*, vol. 433, no. 7027, pp. 725–728, Feb. 2005.

[7] Q. Xu, B. Schmidt, S. Pradhan, and M. Lipson, "Micrometre-scale silicon electro-optic modulator," *Nature*, vol. 435, no. 7040, pp. 325–327, May 2005.

[8] V. Raghunathan, R. Claps, D. Dimitropoulos, and B. Jalali, "Wavelength conversion in silicon using Raman induced four-wave mixing," *Appl. Phys. Lett.*, vol. 85, no. 1, pp. 34–36, Jul. 2004.

[9] Ö. Boyraz, P. Koonath, V. Raghunathan, and B. Jalali, "All optical switching and continuum generation in silicon waveguides," *Opt. Express*, vol. 12, no. 17, pp. 4094–4102, Aug. 2004.

[10] M. Borselli, K. Srinivasan, P. Barclay, and O. Painter, "Rayleigh scattering, mode coupling, and optical loss in silicon microdisks," *Appl. Phys. Lett.*, vol. 85, no. 17, pp. 3693–3695, Oct. 2004.

[11] W. R. Headley, G. T. Reed, S. Howe, A. Liu, and M. Paniccia, "Polarization-independent optical racetrack resonators using rib waveguides on silicon-on-insulator," *Appl. Phys. Lett.*, vol. 85, no. 23, pp. 5523–5525, Dec. 2004.

[12] P. Dumon, W. Bogaerts, V. Wiaux, J. Wouters, S. Beckx, J. V. Campenhout, D. Taillaert, B. Luyssaert, P. Bienstman, D. V. Thourhout, and R. Baets, "Low-loss SOI photonic wires and ring resonators fabricated with deep UV lithography," *IEEE Photon. Technol. Lett.*, vol. 16, no. 5, pp. 1328–1330, May 2004.

[13] V. R. Almeida, C. A. Barrios, R. R. Panepucci, and M. Lipson, "All-optical control of light on a silicon chip," *Nature*, vol. 431, no. 7012, pp. 1081–1084, Oct. 2004.

[14] A. R. Cowan, G. W. Rieger, and J. F. Young, "Nonlinear transmission of 1.5 μm pulses through single-mode silicon-on-insulator waveguide structures," *Opt. Express*, vol. 12, no. 8, pp. 1611–1621, Apr. 2004.

[15] J. I. Dadap, R. L. Espinola, R. M. Osgood, Jr., S. J. McNab, and Y. A. Vlasov, "Spontaneous Raman scattering in a silicon wire waveguide," presented at the Integrated Photonics Research (IPR), San Francisco, CA, Jul. 2004, Paper IWA4.

[16] T. K. Liang and H. K. Tsang, "Pulsed-pumped silicon-on-insulator waveguide Raman amplifier," presented at the Int. Conf. Group IV Photonics, Hong Kong, 2004, Paper WA4.

[17] S. J. Choi, K. Djordjev, S. J. Choi, P. D. Dapkus, W. Lin, G. Griffel, R. Menna, and J. Connolly, "Microring resonators vertically coupled to buried heterostructure bus waveguides," *IEEE Photon. Technol. Lett.*, vol. 16, no. 3, pp. 828–830, Mar. 2004.

[18] S. M. Garner, S.-S. Lee, V. Chuyanov, A. Chen, A. Yacoubian, W. H. Steier, and L. R. Dalton, "Three-dimensional integrated optics using polymers," *IEEE J. Quantum Electron.*, vol. 35, no. 8, pp. 1146–1155, Aug. 1999.

[19] P. Koonath, K. Kishima, T. Indukuri, and B. Jalali, "Sculpting of three-dimensional nano-optical structures in silicon," *Appl. Phys. Lett.*, vol. 83, no. 24, pp. 4909–4911, Dec. 2003.

[20] P. Koonath, T. Indukuri, and B. Jalali, "Vertically-coupled microresonators realized using three-dimensional sculpting in silicon," *Appl. Phys. Lett.*, vol. 85, no. 6, pp. 1018–1020, Aug. 2004.

[21] ——, "Add-drop filters utilizing vertically coupled microdisk resonators in silicon," *Appl. Phys. Lett.*, vol. 86, no. 9, pp. 091102-1–091102-3, Feb. 2005.

[22] T. Indukuri, P. Koonath, and B. Jalali, "Subterranean silicon photonics: Demonstration of buried waveguide-coupled micro-resonators," *Appl. Phys. Lett.* to be published.

[23] M. Chen, X. Wang, J. Chen, X. Liu, Y. Dong, Y. Yu, and X. Wang, "Dose-energy match for the formation of high-integrity buried oxide layers in low-dose separation-by-implantation-of-oxygen materials," *Appl. Phys. Lett.*, vol. 80, no. 5, pp. 880–882, Feb. 2002.

[24] R. A. Soref, E. Cortesi, F. Namavar, and L. Friedman, "Vertically integrated silicon-on-insulator waveguides," *IEEE Photon. Technol. Lett.*, vol. 3, no. 1, pp. 22–24, Jan. 1991.

[25] J. Jiao, B. Johnson, S. Seraphin, M. Anc, R. Dolan, and B. Cordts, "Formation of Si islands in the buried oxide layers of ultra-thin SIMOX structures implanted at 65 keV," *Mater. Sci. Eng.*, vol. 72, no. 2/3, pp. 150–155, Mar. 2000.

[26] J. V. Hryniewicz, P. P. Absil, B. E. Little, R. A. Wilson, and P. T. Ho, "Higher order filter response in coupled microring resonators," *IEEE Photon. Technol. Lett.*, vol. 12, no. 3, pp. 320–322, Mar. 2000.

[27] Y. Yanagase, S. Suzuki, Y. Kokubun, and S. T. Chu, "Box-like filter response and expansion of FSR by a vertically triple coupled microring resonator filter," *J. Lightw. Technol.*, vol. 20, no. 8, pp. 1525–1529, Aug. 2002.

[28] A. Siegman, *Lasers*. Mill Valley, CA: Univ. Science, 1986, ch. 13.

Prakash Koonath received the B.S. degree in physics from Mahatma Gandhi University, Kerala, India, in 1992, the M.Sc. degree in physics from Indian Institute of Technology, Chennai, India, in 1994, the M.Tech. degree in optoelectronics and optical communications from Indian Institute of Technology, New Delhi, India, in 1996, and the Ph.D. degree in electrical engineering from the University of Minnesota, Minneapolis, in 2001.

His doctoral thesis concentrated on the design and development of polarization insensitive semiconductor optical amplifiers and semiconductor laser in III–V material system for both the 1300- and 1550-nm windows. He is currently pursuing a postdoctoral fellowship at the University of California, Los Angeles, where his research is in the area of integrated optical devices in silicon. His research involves the development of novel fabrication technologies to realize devices in silicon and their characterization. His research interests include semiconductor optoelectronics, optoelectronic integration in silicon, and nonlinear optical devices.

Tejaswi Indukuri received the B.Tech. degree in electrical engineering from the Indian Institute of Technology Madras, Chennai, India, in 2000. He is currently working toward the M.S./Ph.D. degrees in electrical engineering at the University of California, Los Angeles.

His interests include silicon photonics, integrated optics/optoelectronics, and semiconductor physics.

Bahram Jalali (S'86–M'89–SM'97–F'04) received the B.S. degree in physics from Florida State University, Tallahassee, in 1984 and the M.S. and Ph.D. degrees in applied physics from Columbia University, New York, NY, in 1986 and 1989, respectively.

He was a member of the Technical Staff at the Physics Research Division of American Telephone and Telegraph Company (AT&T) Bell Laboratories, Murray Hill, NJ, from 1988 to 1993. He joined the Electrical Engineering (EE) Department of the University of California, Los Angeles, in 1993, where he is now a Full Professor. He is the Chair of the Optoelectronic Circuits and Systems Laboratory, Director of the Defense Advanced Research Projects Agency (DARPA) Consortium for Optical A/D System Technology, and former Chair of the Photonic and Optoelectronics Field of Study in the EE Department. He is the Founder of Cognet Microsystems, Los Angeles, which is a fiber-optic component company that was acquired by Intel Corporation in April 2001. He is also involved in the new Biomedical Engineering Interdepartmental Program. His research interests are in radio-frequency photonics, integrated optics, optical communication, and biomedical sensors. He has more than 100 publications and holds six patents.

Dr. Jalali has received the BridgeGate 20 Award for his contribution to the Southern California Economy. He was a Distinguished Lecturer of the Orlando Chapter of the IEEE Lasers and Electrooptics Society (LEOS) in 1998. He was the General Chair of the International microwave photonics (MWP) Conference in 2001, and he served on the technical program committees for the Conference on Lasers and Electrooptics (CLEO) and the Integrated Photonic Research (IPR) Conference.